

# **The subthalamic nucleus contributes causally to perceptual decision-making in monkeys**

Kathryn Rogers, Joshua I. Gold, Long Ding\*

Department of Neuroscience, University of Pennsylvania, Philadelphia, PA 19104

\* Corresponding author ([lding@penncmedicine.upenn.edu](mailto:lding@penncmedicine.upenn.edu))

## 1 **Abstract**

2 The subthalamic nucleus (STN) plays critical roles in the motor and cognitive function of the  
3 basal ganglia (BG), but the exact nature of these roles is not fully understood, especially in the  
4 context of decision-making based on uncertain evidence. Guided by theoretical predictions of  
5 specific STN contributions, we used single-unit recording and electrical microstimulation in the  
6 STN of healthy monkeys to assess its causal, computational roles in visual-saccadic decisions  
7 based on noisy evidence. The recordings identified subpopulations of STN neurons with distinct  
8 task-related activity patterns that related to different theoretically predicted functions.  
9 Microstimulation caused changes in behavioral choices and response times that reflected  
10 multiple contributions to an “accumulate-to-bound”-like decision process, including modulation  
11 of decision bounds and evidence accumulation, and to non-perceptual processes. These results  
12 provide new insights into the multiple ways that the STN can support higher brain function.

13

14

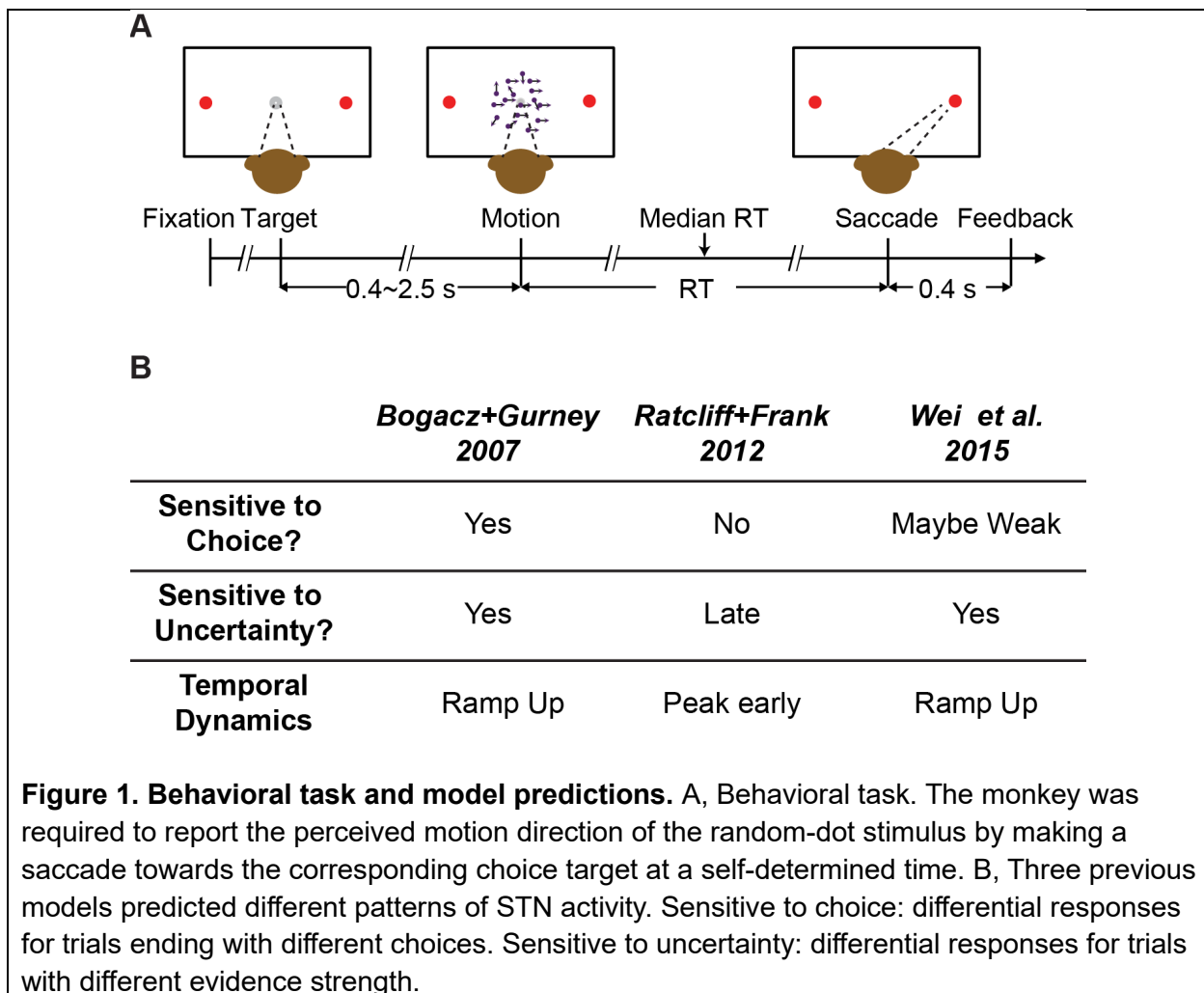
## 15 **Introduction**

16 The subthalamic nucleus (STN) is a critical junction in both the indirect and hyperdirect  
17 pathways of the basal ganglia (BG). It receives inputs from the external segment of the globus  
18 pallidum (GPe) and cortex and sends diffuse excitation to pallidal output nuclei of the BG. The  
19 STN has well-recognized functions in movement control. For example, in humans and monkeys,  
20 lesions of the STN cause involuntary movements of contralateral body parts (Martin, 1927;  
21 Martin and Alcock, 1934; Whittier and Mettler, 1949; Carpenter et al., 1950). In monkeys with  
22 experimentally induced Parkinsonism, STN lesions and inactivation can reverse abnormal BG  
23 output activity and alleviate both akinesia and rigidity (Bergman et al., 1990, 1994; Wichmann et  
24 al., 1994a). In Parkinsonian human patients, deep brain stimulation (DBS) of the STN has  
25 become a common treatment option to alleviate movement abnormalities (DeLong and  
26 Wichmann, 2001).

27 Recognizing that motor symptoms associated with STN damage are often accompanied by  
28 emotional and cognitive deficits, recent work has also begun to examine the roles of the STN in  
29 cognition. For example, the STN has been shown to contribute to cued, goal-driven action  
30 inhibition (Baunez et al., 2001; Desbonnet et al., 2004; Witt et al., 2004; Aron and Poldrack,  
31 2006; Frank et al., 2007; Isoda and Hikosaka, 2008; Schmidt et al., 2013; Pasquereau and Turner,  
32 2017). STN activity can also be sensitive to task complexity and decision conflict, as measured  
33 in imaging studies and human patients undergoing DBS (Lehericy et al., 2004; Aron et al., 2007;  
34 Fumagalli et al., 2011; Brittain et al., 2012; Zaghoul et al., 2012; Zavala et al., 2017). These  
35 findings have led to the idea that STN may also contribute to resolving difficult decisions based  
36 on uncertain evidence. This idea has been formalized in several computational models, which  
37 posit three, not mutually exclusive, functions for STN: 1) through its interaction with GPe, STN  
38 computes a normalization signal to calibrate how the available, alternative options are assessed  
39 (Bogacz and Gurney, 2007; Coulthard et al., 2012; Green et al., 2013); 2) in coordination with  
40 the medial prefrontal cortex, STN adjusts decision bounds (i.e., thresholds on accumulated

41 evidence that govern decision termination and commitment) to control impulsivity in responding  
 42 (Frank, 2006; Cavanagh et al., 2011; Ratcliff and Frank, 2012; Zavala et al., 2014; Herz et al.,  
 43 2016, 2017; Pote et al., 2016); and 3) by maintaining the balance between the direct and indirect  
 44 pathways of the BG, STN helps to implement a nonlinear computation that improves the efficacy  
 45 with which the BG adjusts decision bounds (Lo and Wang, 2006; Wei et al., 2015).

46 Guided by predictions of these models (Figure 1B), we assessed the role of the STN in decisions  
 47 made by monkeys performing a random-dot visual motion direction discrimination task (Figure.  
 48 1A). We recorded from individual STN neurons while monkeys performed the task and found  
 49 activity patterns that were highly heterogenous across neurons. Nevertheless, these patterns  
 50 could be sorted into three prominent clusters with functional properties that, in principle, could  
 51 support each of the three theoretically predicted STN functions from previous modeling studies.  
 52 In addition, we tested STN's causal contribution to the decision process using electrical  
 53 microstimulation. These perturbations of STN activity affected both choice and reaction time  
 54 (RT) performance in multiple ways that could be ascribed to particular computational  
 55 components of an “accumulate-to-bound” decision process. As detailed below, these results show  
 56 that STN can play multiple, causal roles in the formation of a deliberative perceptual decision,



57 likely reflecting its diverse contributions to the many cognitive and motor functions that depend  
58 on the BG.

## 59 **Results**

### 60 ***STN neurons show diverse response profiles***

61 We recorded 203 neurons while the monkeys were performing a random-dot motion  
62 discrimination task ( $n = 115$  and  $88$  for monkeys C and F, respectively). The behavioral  
63 performance of both monkeys has been documented extensively (Ding and Gold, 2010, 2012a;  
64 Fan et al., 2018). Their performance in three example sessions are shown in Figure 4A–C (black  
65 data points). In general, both monkeys made more contralateral choices with increasing signed  
66 motion strength (positive for motion toward the contralateral target) and had lower RTs (i.e.,  
67 faster responses) for higher absolute motion strength.

68 STN neurons showed diverse response profiles. Figure 2A shows average activity patterns of  
69 three example neurons. The top neuron showed an initial suppression of activity after motion  
70 onset and became active, in a choice-dependent manner, before saccade onset. The middle  
71 neuron showed choice- and motion coherence-dependent activation during the motion-viewing  
72 period before saccade onset. The bottom neuron exhibited activation after motion onset that was  
73 similar for both choices and all coherence levels, which then decayed in a choice- and coherence-  
74 dependent manner around saccade onset.

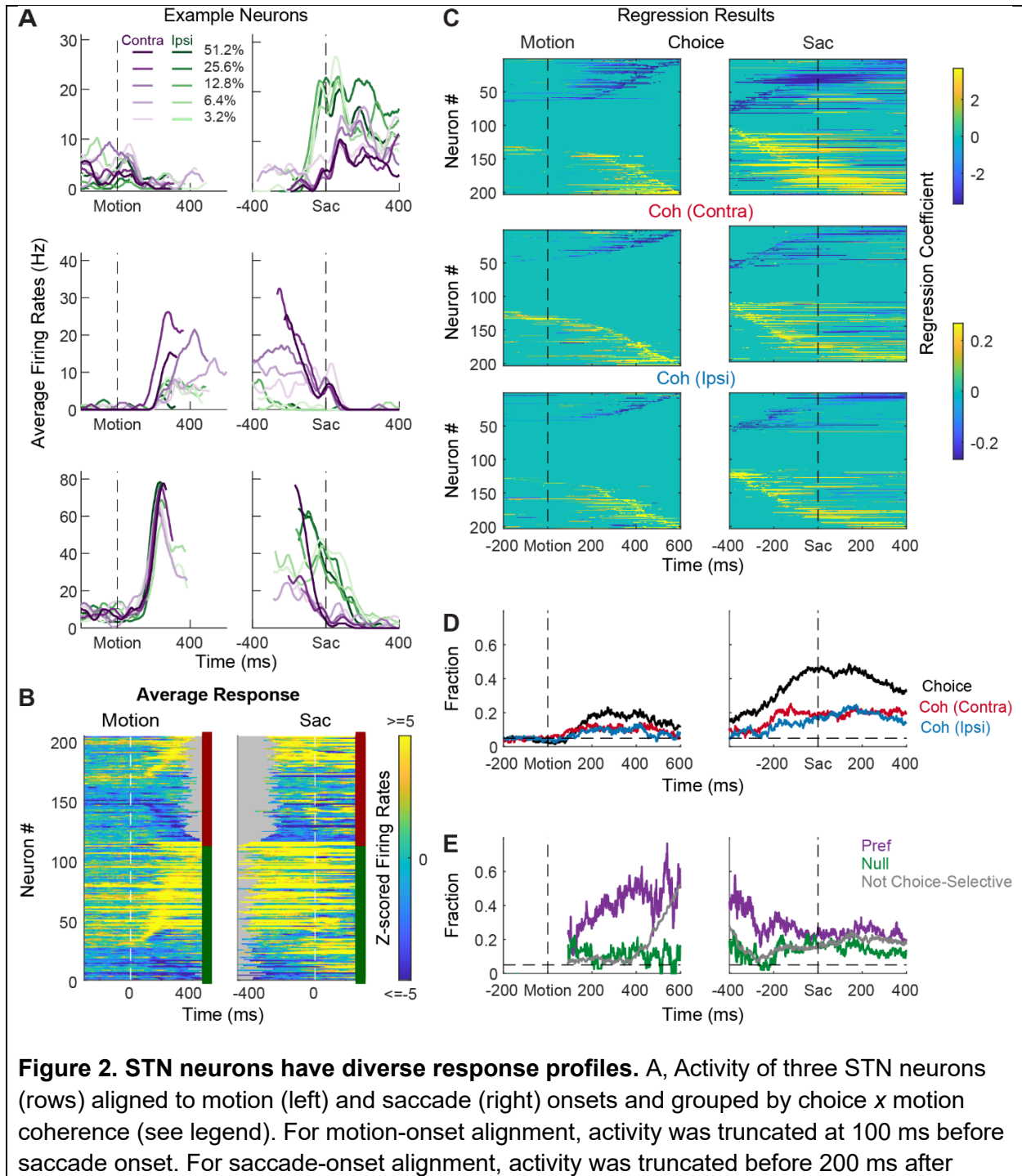
75 The diversity of response profiles can be seen in the summary heatmaps for the population  
76 (Figure 2B). When activity was averaged across all trial types, STN neurons can become  
77 activated or suppressed (warm vs. cool colors, respectively), relative to pre-stimulus baseline,  
78 during motion viewing and around saccade onset. The timing of peak modulation also spanned  
79 the entire motion-viewing period and extended beyond saccade generation, including a  
80 substantial fraction of neurons that also responded to target onset before the motion stimulus  
81 appeared. These diverse spatiotemporal response profiles suggest that the STN as a whole may  
82 serve multiple functions in perceptual decision-making.

83 Across the population, a substantial fraction of neurons was sensitive to choice, motion  
84 coherence, and RT (Figure 2C–E, Supplementary Figure 1). We performed multiple linear  
85 regressions, separately for coherence and RT (Eqs. 1 and 2), for each neuron and used the  
86 regression coefficients to measure these decision-related sensitivities. For choice sensitivity  
87 (Figure 2C, first row), both contralateral and ipsilateral preferences were commonly observed.

88 The overall fraction of neurons showing choice sensitivity increased after motion onset and  
89 peaked at saccade onset (Figure 2D). For coherence sensitivity, modulations were observed for  
90 trials with contralateral or ipsilateral choices and with similar tendencies for positive and  
91 negative coefficients (Figure 2C, rows 2 and 3). The fraction of neurons showing reliable  
92 coherence sensitivity was also higher around saccade onset (Figure 2D).

93 Despite the diverse distributions of regression coefficients, there were systematic patterns in  
94 when and how these forms of selectivity were evident in the neural responses. Notably, neurons  
95 showing choice sensitivity were more likely to show coherence modulation during early motion

96 viewing, especially for trials when the monkey chose the neuron's preferred choice (Figure 2E,  
 97 purple). In contrast, coherence modulation emerged later for neurons that did not show choice  
 98 sensitivity (Figure 2E, gray lines). These systematic interactions in modulation types suggest that  
 99 the STN population does not simply reflect a random mix of selectivity for decision-related  
 100 quantities. Instead, there appears to exist subpopulations with distinct decision-related  
 101 modulation patterns, which we detail below.



motion onset. B, Summary of average activity patterns. Each row represents the activity of a neuron, z-scored by baseline activity in a 300 ms window before target onset and averaged across all trial conditions. Rows are grouped by monkey (red and green shown to the right of each panel: monkeys C and F, respectively) and sorted by the time of peak values relative to motion onset. Only correct trials were included. C, Heatmaps of linear regression coefficients for choice (top), coherence for trials with contralateral choices (middle), and coherence for trials with ipsilateral choices (bottom), for activity aligned to motion (left) and saccade (right) onsets. Regression was performed in running windows of 300 ms. Regression coefficients that were not significantly different from zero ( $t$ -test,  $p > 0.05$ ) were set to zero (green) for display purposes. Neurons were sorted in rows by the time of peak coefficient magnitude. Only correct trials were included. D, Time courses of the fractions of regression coefficients that were significantly different from zero ( $t$ -test,  $p < 0.05$ ), for choice (black), coherence for trials with contralateral choices (red), and coherence for trials with ipsilateral choices (blue). Dashed line indicates chance level. E, Time courses of the fractions of non-zero regression coefficients for coherence. Separate fractions were calculated for trials with the preferred (purple) and null (green) choices from choice-selectivity activity and for all trials from activity that was not choice selective (gray). Only time points after motion onset with fractions  $> 0.05$  for choice-selective activity were included. Dashed line: chance level.

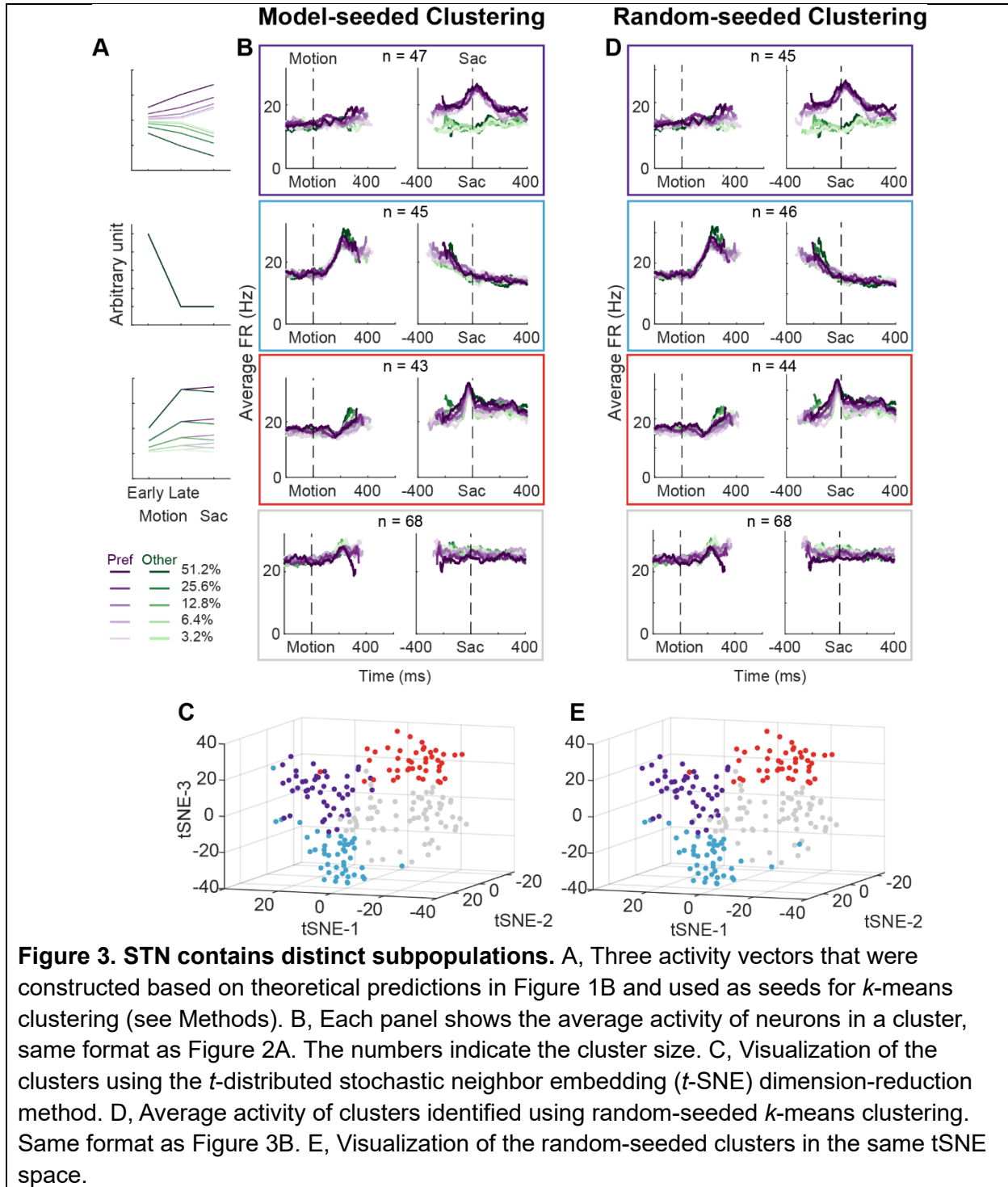
102

### 103 **STN subpopulations can support previously theorized functions**

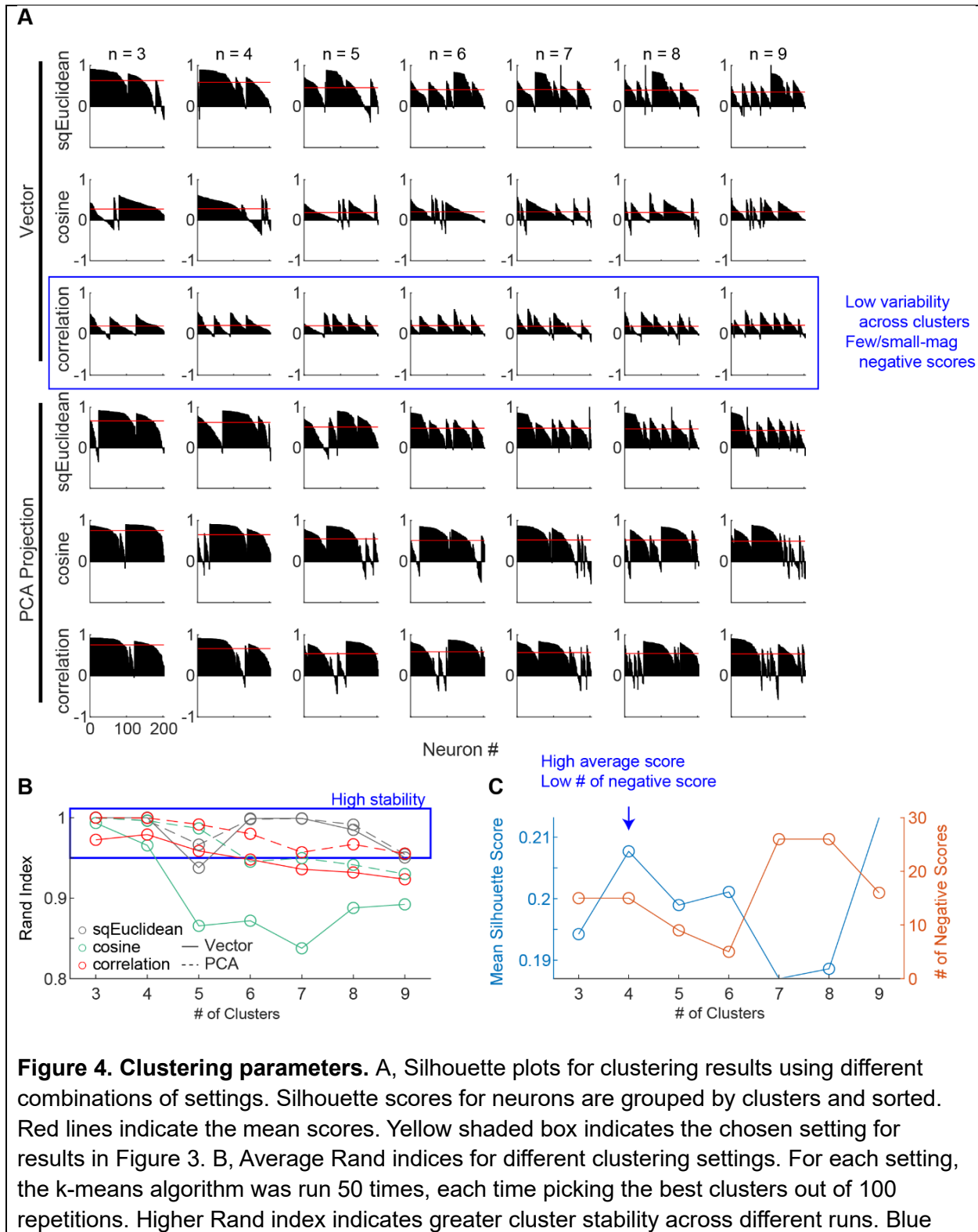
104 Using two forms of cluster analysis, we identified three subpopulations of neurons in the STN  
105 with distinct activity patterns that conform to predictions of each of the three previously  
106 published sets of models. For the first analysis, we represented a neuron's activity pattern with a  
107 30-dimension vector, consisting of normalized average activity associated with two choices, five  
108 coherence levels, and three task epochs. We generated three artificial vectors based on the  
109 predicted activity patterns of each model, as follows (Figure 3A). Bogacz and Gurney (2007)  
110 posited that STN neurons, through their reciprocal connections with the external segment of  
111 globus pallidum, pool and normalize evidence-related signals, leading to the prediction of choice  
112 and coherence-modulated activity during motion viewing (Figure 3A, top; based on simulations  
113 using equations in their Appendix B). Ratcliff and Frank (2012) posited that STN neurons,  
114 through their direct innervation by cortical regions, provide an early signal to suppress immature  
115 choices, leading to the prediction of a choice-independent signal that appears soon after motion  
116 onset and dissipates over time (Figure 3A, middle; based on their Figure 5). Wei and colleagues  
117 (2015) posited that the STN balances evidence-related signals in the GPe until near decision  
118 time, leading to the prediction of coherence-dependent ramping activity with no or weak choice  
119 selectivity (Figure 3A, bottom; based on their Figure 2D). We performed k-means clustering  
120 using these three vectors and another arbitrary vector as the seeds to group the population into  
121 four clusters.

122 Figure 3B shows the average activity from each of the resulted clusters. Consistent with the  
123 design of this analysis, the first cluster tends to show choice- and coherence-dependent activity  
124 that also ramps up during motion viewing (Figure 3B, first row,; Supplementary Figure 2). The  
125 second cluster tends to show an early, sharper rise in activity during motion viewing and this

126 activity gradually decreases toward saccade onset (Figure 3B, second row). The third cluster  
 127 tends to show ramping activity during motion viewing with similar coherence modulation for  
 128 both choices and a short burst of activity for one choice just before saccade onset (Figure 3B,  
 129 third row; Supplementary Figure 2). The last cluster shows mixed and, on average, weak task-  
 130 related modulation (Figure 3B, bottom row; Supplementary Figure 2B). The first three clusters



131 contained similar numbers of neurons. When visualized using the T-distributed stochastic  
 132 neighbor embedding technique, these clusters did not form a single continuum but instead  
 133 reflected separable features between clusters (Figure 3C). In other words, the clustering did not





box indicates settings with Rand indices > 0.95. C, Mean silhouette scores and the number of negative scores as a function of number of clusters, using the firing rate vectors and correlation distance. Higher mean score and fewer negative scores indicate better clustering.

134 simply force a uniform distribution with random-mixed selectivity into four groups.

135 For the second cluster analysis, we used random seeds without considering any of the model  
136 predictions and obtained almost identical clusters. As detailed in Methods, we explored a wide  
137 range of settings for clustering, including: 1) using directly the 30-D vectors or their principal  
138 component projections, 2) basing the clustering on three different distance metrics, and 3)  
139 varying the number of presumed clusters. To identify the best setting, we assessed the goodness  
140 of clustering using the silhouette score and the stability of clustering using the Rand index (Rand,  
141 1971) (Figure 4). The silhouette score quantifies for each member the relative distance between  
142 its average within-cluster distance and distance to those in its closest neighboring cluster (a  
143 higher score indicates better cluster separation). The silhouette plots favored the combination of  
144 using the 30-D vector directly and correlation distance (Figure 4A, third row), which generated  
145 less variability across clusters and few/small-magnitude negative silhouette scores (negative  
146 scores indicate that a member is closer to its neighboring cluster than its own cluster).

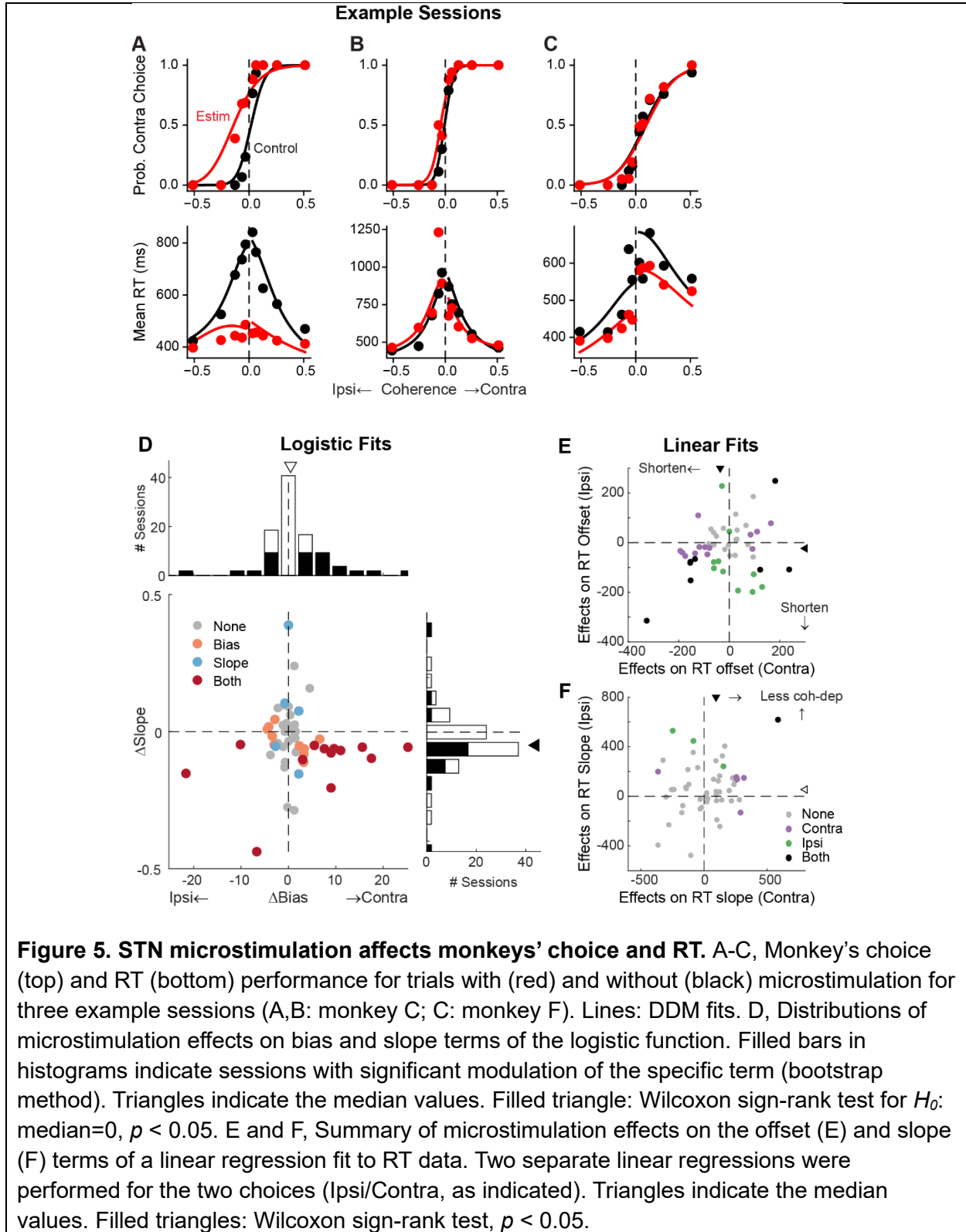
147 The Rand index measures how consistently two members are assigned to the same clusters from  
148 different iterations of clustering (a high index indicates greater stability). The Rand index was  
149 generally high (above 0.95 out of a max of 1; blue box) except for the combination of using the  
150 30-D vector and cosine distance (Figure 4B). Finally, using the raw vector-correlation  
151 combination, an assumption of four clusters resulted in the highest average Rand index and  
152 assuming 4-6 clusters generally resulted in higher mean silhouette score and lower number of  
153 negative scores (Figure 4C; blue arrow). We thus considered that the raw-vector-correlation  
154 combination and an assumption of four clusters produced the most stable and plausible results.

155 As shown in Figure 3D and E, the four clusters thus identified closely matched those obtained  
156 using model predicted seeds, in terms of the average activity, the cluster sizes, and their locations  
157 in the tSNE space. Increasing the assumed number of clusters caused changes mostly in the gray  
158 cluster, with some changes in the blue cluster, and little effects on the red and purple clusters  
159 (Supplementary Figures 3 and 4). Together these results suggest that, absent the ground truth on  
160 the number of subpopulations in STN, there exist at least three subpopulations that each  
161 corresponds to the predictions of one of three previous published models. As a consequence,  
162 STN appears in principle to be able to support multiple decision-related functions.

163

### 164 **Perturbation of STN activity affects choice and RT**

165 To better understand STN's functional roles in the decision process, we perturbed STN activity  
166 using electrical microstimulation while monkeys performed the task. Specifically, we applied a  
167 train of current pulses at identified STN sites during decision formation, lasting from motion  
168 onset to saccade onset. Figure 5 shows microstimulation effects on choices and RTs in three  
169 example sessions. In the first example session, STN microstimulation caused a leftward



170 horizontal shift (more contralateral choices) and slope reduction (more variable choices) in the  
 171 psychometric curve (Figure 5A, top), as well as a substantial flattening of RT curves (faster

172 responses that depended less on motion coherence) for both choices (bottom). In the second  
173 example session, STN microstimulation induced a minor leftward shift in the psychometric curve  
174 and asymmetric changes in RT for the two choices (Figure 5B). In the third example session,  
175 STN microstimulation did not change the psychometric curve but caused reductions in RT for  
176 both choices (Figure 5C).

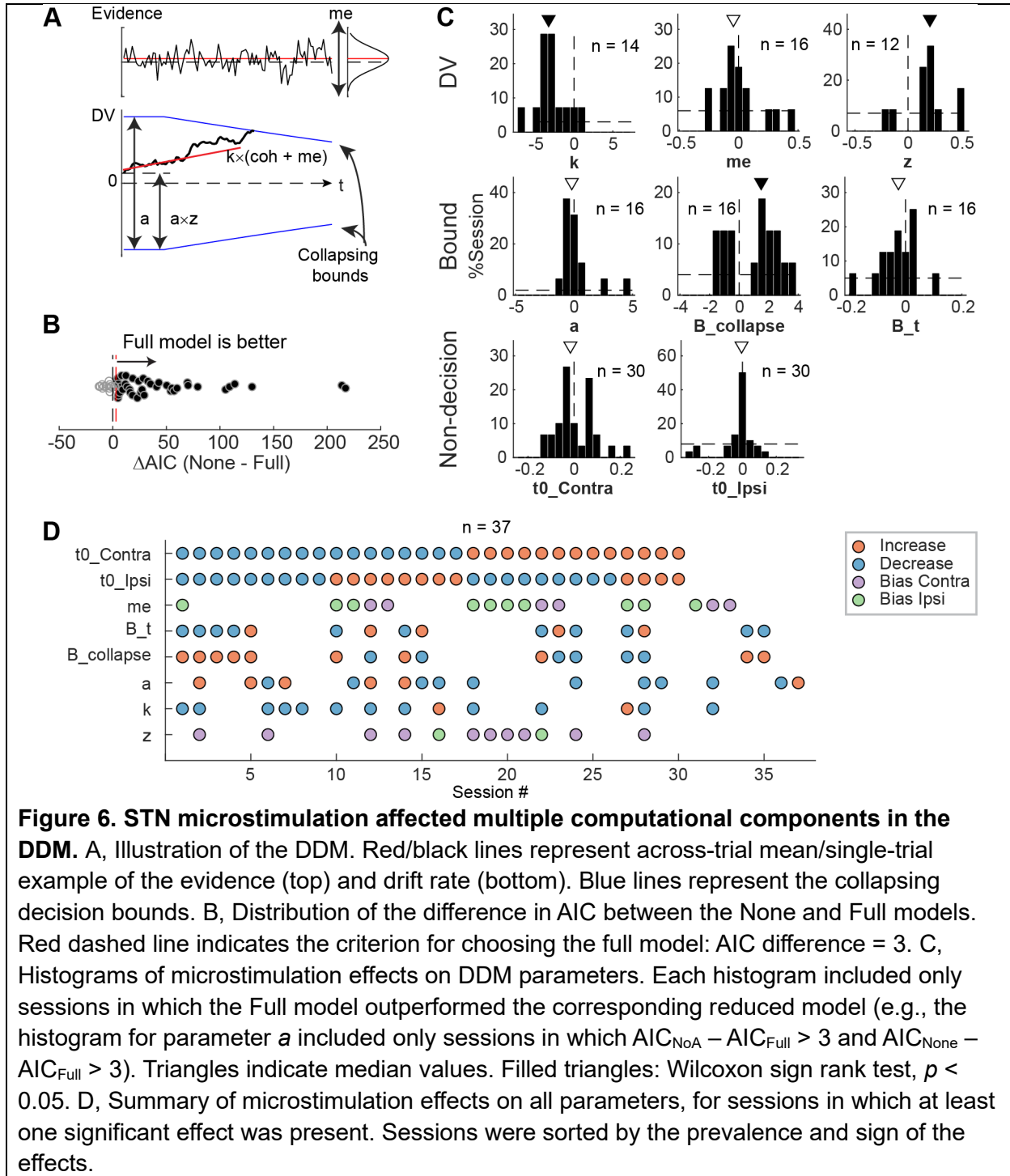
177 Across 54 different STN sites, microstimulation caused variable choice biases and tended to  
178 reduce the dependence of choice on motion strength. We fitted the choice data to a logistic  
179 function and measured choice bias (horizontal shift) and motion strength-dependence (slope). In  
180 23 sessions, microstimulation induced a reliable choice bias (Figure 5D). The induced bias was  
181 toward the contralateral or ipsilateral choice in 15 and 8 sessions, respectively, and the median  
182 value for bias was not significantly different from zero (Wilcoxon sign-rank test,  $p = 0.15$ ). In 18  
183 sessions, microstimulation induced a change in the slope. The slope was reduced in 15 sessions  
184 and the median value was negative ( $p = 0.008$ ). These tendencies were robust across different  
185 variants of logistic functions, with or without lapse terms to capture errors independent of motion  
186 strength (Supplementary Figure 5). Of the sessions where inclusion of lapse terms for the control  
187 and microstimulation trials produced lower AICs, very few showed significant microstimulation-  
188 induced changes in lapses (2 sessions each for the “Symmetric Lapse” and “Asymmetric Lapse”  
189 variants). Thus, based on fitting results using logistic functions, STN microstimulation most  
190 consistently reduced the choice dependence on motion strength, caused session-specific choice  
191 biases, and had minimal effects on lapses.

192 Microstimulation also tended to reduce RT. We fitted linear functions separately for RTs  
193 associated with the two choices, in which offset and slope terms measure coherence-independent  
194 and -dependent changes in RTs, respectively. Microstimulation caused changes in RT offsets in  
195 25 sessions for contralateral choices (18 were reductions in RT, with a median change across all  
196 sessions of -36 ms; Wilcoxon sign-rank test for  $H_0$ : median change=0,  $p < 0.0001$ ) and 18  
197 sessions for ipsilateral choices (15 reductions, mean change = -23 ms,  $p < 0.0001$ ; Figure 5E).  
198 Microstimulation caused changes in RT slopes in 6 sessions for contralateral choices (5 were  
199 positive, implying a weaker coherence dependence;  $p < 0.0001$ ) and 4 sessions for ipsilateral  
200 choices (all 4 were positive; Figure 5F). Thus, based on fitting results using linear functions,  
201 STN microstimulation can induce choice-specific changes in RT, with overall tendencies to  
202 reduce both the coherence-independent component and the RT’s dependence on coherence for  
203 the contralateral choice.

204

### 205 **Microstimulation effects reflected changes in multiple computational components**

206 To infer STN’s computational roles in the decision process, we examined the microstimulation  
207 effects using a drift-diffusion model (DDM) framework. This framework has been widely used in  
208 studies of perceptual decision-making and can provide a unified, computational account of both  
209 choice and RT (Gold and Shadlen, 2007). It assumes that noisy evidence is accumulated over  
210 time and a decision is made when the accumulated evidence reaches a certain decision bound.  
211 The overall RT is the sum of the time needed to reach the bound and non-decision times



212 reflecting perceptual and motor latencies. Previous theoretical models also made predictions  
213 about the effects of perturbing STN activity that can be interpreted in the DDM framework. The

214 model by Bogacz and Gurney (2007) predicted that the perturbation would reduce the effect of  
215 task difficulty on decision performance by eliminating a nonlinear transformation that is needed  
216 for appropriate evidence accumulation (Green et al., 2013). The model by Ratcliff and Frank

217 (2012) predicted that the perturbation, by causing changes in the STN's influence onto the  
218 substantia nigra pars reticulata (SNr), would change temporal dynamics of the decision bound  
219 and influence non-decision time. The model by Wei and colleagues (2015) predicted that the  
220 perturbation would result in a reduction in the decision bound.

221 To test whether these predictions, and/or other effects, were present in our microstimulation data,  
222 we fitted a DDM to choice and RT data simultaneously (Figure 6A). We performed AIC-based  
223 model selection and found that, in 40 of 54 sessions, the Full model, which included  
224 microstimulation effects on any model parameters, outperformed the None model, which  
225 assumed that there was no microstimulation effect on any parameters (Figure 6B). This result  
226 implies that, in these sessions, STN microstimulation affected one or more computational  
227 components of the decision process. To better characterize these effects, we compared AICs  
228 between the Full model and six reduced models to identify sessions with reliable  
229 microstimulation-induced changes in particular model parameters (Supplementary Figure 6A).

230 We found that STN microstimulation resulted in reliable changes in several model parameters  
231 over different subsets of sessions (Figure 6C and D). Consistent with model predictions from  
232 Bogacz and Gurney (2007), microstimulation reduced the scale factor for evidence  
233 accumulation,  $k$ , in 14 sessions. This effect contributed to a decreased motion coherence  
234 dependence of choice and RT (Figure 6C, first histogram; Wilcoxon sign-rank test for  $H_0$ : zero  
235 median effect,  $p = 0.021$ ). Consistent with model predictions from Ratcliff and Frank (2012) and  
236 Wei and colleagues (2015), microstimulation affected parameters that controlled the decision  
237 bound ( $a$ ,  $B\_collapse$ ,  $B\_t$ ) in 16 sessions each (not necessarily in the same sessions for each  
238 parameter, see Figure 6D). The changes in the maximal decision bound ( $a$ ) were variable across  
239 sessions ( $p = 0.68$ ). The changes in the collapsing bound dynamics ( $B\_collapse$ ,  $B\_t$ ) tended to  
240 indicate faster and earlier decreases in bounds ( $p = 0.039$  and  $0.088$ , respectively). Consistent  
241 with model predictions from Ratcliff and Frank (2012), microstimulation caused changes in non-  
242 decision times in 30 sessions ( $t0\_Contra$  and  $t0\_Ipsi$ ). These changes varied from session to  
243 session ( $p = 0.28$  and  $0.75$ , respectively). Statistical tests on fitted parameters of all sessions,  
244 regardless of whether a microstimulation effect was necessary to account for the behavioral data,  
245 showed similar trends (Supplementary Figure 6B).

246 STN microstimulation had two additional effects beyond those predicted by the previous  
247 modeling studies. First, consistent with the above-demonstrated microstimulation-induced choice  
248 biases (Figure 5), microstimulation induced offsets in momentary ( $me$ ;  $n = 16$  sessions;  $p = 0.61$ )  
249 and accumulated ( $z$ ;  $n = 12$  sessions;  $p = 0.016$ ) evidence. Second, the microstimulation effects  
250 involved changes in more than one model parameter in the majority of sessions (Figure 6D). We  
251 did not observe any dominant combinations of effects. These results suggest that the STN is  
252 causally involved in multiple decision-related functions, including those mediating the  
253 dependence on evidence, choice biases, and bound dynamics.

254

255 **Distribution of microstimulation effects reflected intermingled neuron activity patterns**

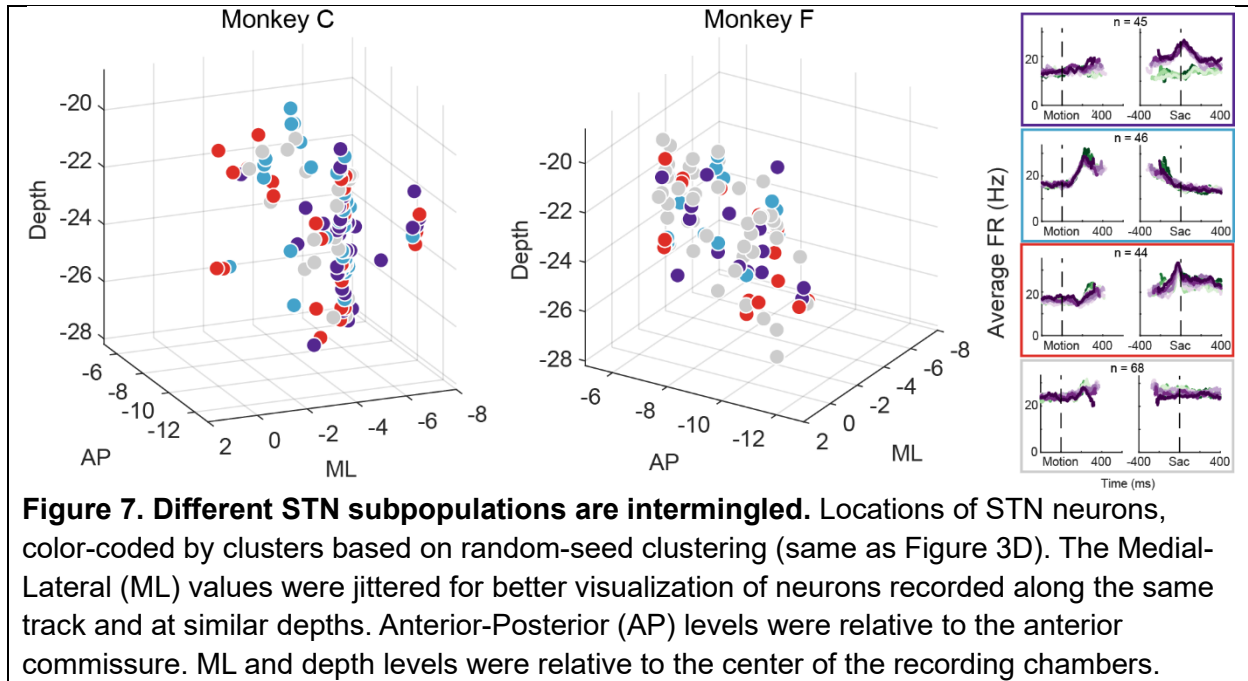
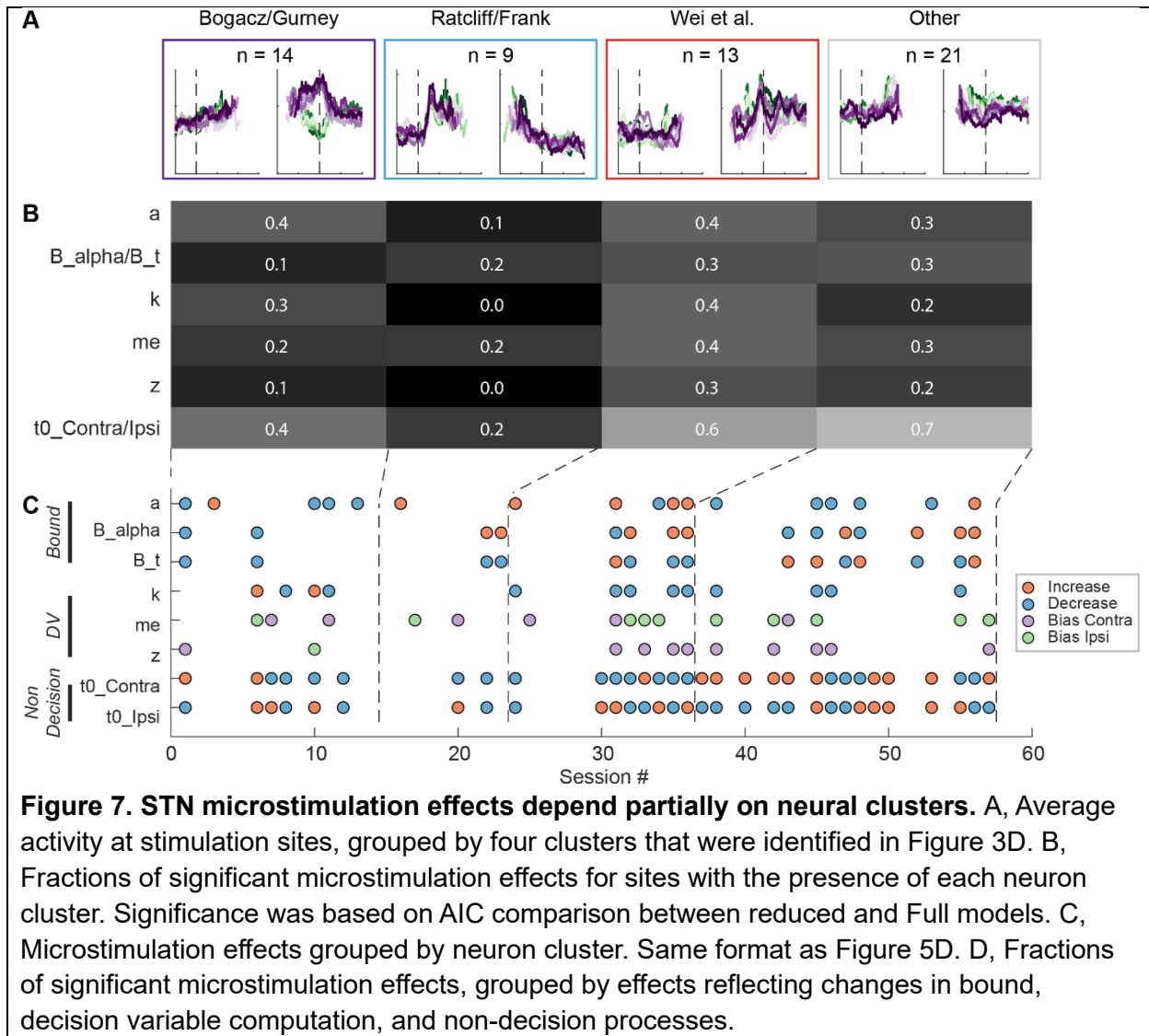


**Figure 7. Different STN subpopulations are intermingled.** Locations of STN neurons, color-coded by clusters based on random-seed clustering (same as Figure 3D). The Medial-Lateral (ML) values were jittered for better visualization of neurons recorded along the same track and at similar depths. Anterior-Posterior (AP) levels were relative to the anterior commissure. ML and depth levels were relative to the center of the recording chambers.

256 The multi-faceted microstimulation effects, combined with the fact that the kind of  
257 microstimulation we used tends to activate not just one neuron, but rather groups of neurons near  
258 the tip of the electrode (Tehovnik, 1996), suggested that STN neurons with different functional  
259 roles are located close to one another. Consistent with this idea, neurons that were classified as  
260 belonging to different clusters tended to be intermingled (Figure 7). We did not observe any  
261 consistent topographical organization patterns within or between the two monkeys. At certain  
262 locations, neurons belonging to different clusters were recorded using the same electrode. We  
263 calculated silhouette scores to quantify whether the activity pattern-based neuron clusters also  
264 formed clusters in the 3D physical space. The mean values were -0.09 and -0.11 for the two  
265 monkeys, respectively, indicating that neurons were often closer to others from a different cluster  
266 than those within the same cluster. In other words, STN subpopulations did not segregate from  
267 each other and instead tended to be intermingled, and thus microstimulation likely activated  
268 multiple neurons with different functional properties.

269 Although the intermingled organization of STN subpopulations, defined based on their task-  
270 related activity patterns (Figure 3), made it challenging to relate a specific microstimulation  
271 effect to a specific subpopulation, we did observe certain trends that could contribute to the site-  
272 specific microstimulation effects. We assigned the single or multi-unit activity at the stimulation  
273 sites according to the clusters identified using the random-seeded clustering (Figure 8A). We  
274 then grouped the sites by neuron clusters (Figure 8C). When neurons of different clusters were  
275 recorded at the same site, the same microstimulation effects were assigned to each cluster. We  
276 found that the second cluster was associated with lower overall likelihood of observing  
277 microstimulation effects compared to other clusters (Figure 8B; Chi-square test,  $H_0$ : the  
278 likelihood is the same for the first cluster and the other clusters;  $p = 0.003$ ), while the third  
279 cluster had higher overall likelihood ( $p = 0.035$ ). For the first three clusters, no microstimulation



280 effect dominated ( $p > 0.3$  for all), whereas it was more likely to observe effects on non-decision  
 281 times for the fourth cluster (i.e., with neural activity patterns not related to the three models;  $p =$   
 282 0.001).

283 The sign of microstimulation effects depended weakly on neuron clusters. For example, it was  
 284 more likely to observe an increase in maximal bound height (“a”) for the third neuron cluster  
 285 (Chi-square test,  $H_0$ : same fractions of increase/decrease for all clusters;  $p = 0.073$ ; Chi-square  
 286 test,  $H_0$ : equal fractions of increase/decrease within the cluster;  $p = 0.036$ ). Microstimulation  
 287 decreased the scale factor (“k”) for the third and fourth clusters but caused variable changes for  
 288 the first cluster ( $p = 0.070$  and  $0.021$ , respectively). Microstimulation effects on the non-decision  
 289 time for the contralateral choices were dominated by increases for the fourth cluster ( $p = 0.04$   
 290 and  $0.007$ , respectively). Together, these results suggested that microstimulation effects reflected  
 291 multiple contributions of intermingled STN subpopulations to decision- and non-decision-related  
 292 processes.

293 **Heterogeneous activity patterns and microstimulation effects cannot be explained by**  
294 **variations in motivational state**

295 Another potential source of heterogeneity in our data may reflect variations in the monkeys'  
296 motivational state across sessions. In two sets of analyses, we did not observe any significant  
297 influence of motivational state on the recording or microstimulation data. For these analyses, we  
298 used the rate of fixation break, overall error rate, and mean RT as indices of motivational state.  
299 None of these measurements differed among sessions when different subpopulations were  
300 encountered (Supplemental Figure 7), suggesting that the motivational state cannot predict which  
301 type of activity pattern would be observed. Similarly, none of these measurements significantly  
302 correlated with the microstimulation effects in any DDM component (Supplemental Table 1),  
303 suggesting that the motivational state did not modulate the magnitude of microstimulation  
304 effects. Together, these results suggest that the diverse activity patterns and microstimulation  
305 effects cannot be accounted for by variations in the monkeys' task engagement.

306 **Discussion**

307 We provide the first characterization of single-unit recordings and electrical microstimulation in  
308 the STN of monkeys performing a demanding perceptual-decision task. We show that: 1) STN  
309 neurons are heterogeneous in their response profiles; 2) different STN subpopulations, with  
310 distinct decision-related activity modulation patterns and intermingled within the region, can  
311 support previously-theorized functions; and 3) electrical microstimulation in STN causes  
312 changes in choice and RT behaviors, reflecting effects on multiple computational components of  
313 an accumulate-to-bound decision process. These results indicate that the STN plays important  
314 and complex roles in perceptual decision formation, both supporting and extending existing  
315 views of STN function.

316 Our study was motivated by the differing predictions of STN activity patterns from several  
317 theoretical studies that were based on STN cellular physiology, connectivity, and/or response  
318 patterns in non-perceptual decision-making contexts (Bogacz and Gurney, 2007; Ratcliff and  
319 Frank, 2012; Wei et al., 2015). Remarkably, we found three clusters of STN activity that are  
320 consistent with each of these predictions. The three clusters were robust and stable, emerging  
321 when we used two different clustering methods (one with model-based seeds, the other with  
322 random seeds). Interestingly, Zavala and colleagues (2017) have reported two types of STN  
323 responses in human patients performing a flanker task. The "early" response they identified may  
324 correspond to our second cluster, while the "late" response may reflect a combination of our first  
325 and third clusters. Together these results suggest that the primate STN contains distinct  
326 subpopulations with different functional roles. Combined with the microstimulation results, the  
327 presence of these subpopulations suggests that the STN can both contribute to the conversion of  
328 sensory evidence into an appropriately formatted/calibrated decision variable and modulate the  
329 dynamics of decision bound. Future studies of BG function should strive to better understand  
330 how these subpopulations interact with each other, as well as with other neurons in the BG and  
331 the larger decision network to support decision making.



332 Despite the general agreements between our observations and previous theoretical predictions,  
333 there were also differences that could be informative for developing future BG models. Most  
334 notably, previous models focused on the period of evidence accumulation and less on neural  
335 activity patterns at or after decision commitment. In contrast, our data show interesting  
336 modulations around saccade onset (see Figure 3) that raise several intriguing possibilities for  
337 STN's contributions to the decision process. In particular, one subpopulation showed a broad  
338 peak with strong choice modulation and little coherence modulation. These modulations may  
339 reflect bound-crossing in an accumulate-to-bound process (but see below). A second  
340 subpopulation returned to the baseline level before saccade onset. The relatively constant  
341 trajectory of this modulation may reflect a collapsing bound or urgency signal that is dependent  
342 only on elapsed time and not the sensory evidence. A third subpopulation maintained coherence-  
343 dependent activity until very close to saccade onset and showed a sharp peak with little choice or  
344 coherence modulation. This sharp peak may signal the end of decision deliberation, without  
345 specifying which decision is made, to direct the network to a post-decision state for decision  
346 evaluation.

347 The diverse activity patterns and their intermingled distribution in the STN underscore the  
348 challenge of identifying specific, causal contributions of a particular neural subpopulation. In  
349 many sessions, we observed effects that have been predicted theoretically and observed  
350 experimentally in human PD patients undergoing DBS. These effects included a reduction in RT,  
351 a weaker dependence on evidence, and changes in the maximal value and trajectories of the  
352 decision bound (Frank et al., 2007; Cavanagh et al., 2011; Coulthard et al., 2012; Green et al.,  
353 2013; Zavala et al., 2014; Herz et al., 2016; Pote et al., 2016). In addition to these previously  
354 observed effects, microstimulation also changed choice biases, measured as horizontal shifts of  
355 psychometric functions and as two different types of biases in the DDM framework. This  
356 departure from previous DBS studies may arise from different task designs (button press versus  
357 eye movement), health status of the subjects, and experience level (minimally versus extensively  
358 trained). The lateralized bias suggests that the STN may be involved in flexible decision  
359 processes that adapt to environments with asymmetric prior probability and/or reward outcomes  
360 for different alternatives, in addition to modulating speed-accuracy tradeoff. Consistent with this  
361 idea, DBS can affect the threshold for deliberations over uncertain sensory inputs or motivational  
362 factors such as reward and effort (Pagnier et al., 2024), suggesting that the STN may be part of a  
363 general selection machinery that can incorporate sensory evidence with information about the  
364 task environment (Redgrave et al., 1999).

365 The intermingled subpopulations may appear at odds with the conventional idea of topography in  
366 how the STN is organized. For example, the “tripartite model” suggests that STN is segregated  
367 by motor, associative, and limbic functions (Parent and Hazrati, 1995); afferents from motor  
368 cortices and neurons related to different types of movements are largely somatotopically  
369 organized in the STN (DeLong et al., 1985; Nambu et al., 1996); and certain molecular markers  
370 are expressed in an orderly pattern in the STN (reviewed in Prasad and Wallén-Mackenzie,  
371 2024). Because we focused on STN neurons that were responsive on a single oculomotor  
372 decision task, our sampling was likely biased toward STN subdivisions related to associative  
373 function and oculomotor movements. As such, our results do not preclude the presence of

374 topography at a larger scale. Rather, our results underscore the importance of activity pattern-  
375 based analysis, in addition to anatomy-based analysis, for understanding the functional  
376 organization of the STN.

377 Our findings also suggest that STN's role in decision formation differs in important ways from  
378 other oculomotor regions that have been examined under similar conditions. First, in the frontal  
379 eye field (FEF), lateral intraparietal area (LIP), and superior colliculus (SC), decision-related  
380 neural activity is dominated by a choice- and coherence-dependent “ramp-to-bound” pattern  
381 (Roitman and Shadlen, 2002; Ding and Gold, 2012a; Crapse et al., 2018; Cho et al., 2021; Jun et  
382 al., 2021; Stine et al., 2023), with additional multiplexing of decision-irrelevant signals (Meister  
383 et al., 2013). In contrast, different STN subpopulations can carry distinct signals that may all be  
384 relevant to decision formation. Moreover, these signals include patterns not evident in the other  
385 regions, such as a choice- and coherence-independent activation in early motion viewing (blue  
386 cluster in Figure 3B and D), that may signal a unique role for the STN.

387 Second, choice-selective ramping activity has been identified in LIP, FEF, SC, the caudate  
388 nucleus, and now two STN subpopulations (Ding and Gold, 2010; Fan et al., 2020). However,  
389 such activity differs among these oculomotor regions just before saccade onset for the preferred  
390 choice. In LIP, FEF, and SC, when the ramping activity is aligned to saccade onset, it shows  
391 negative coherence modulation and positive RT modulation before converging to a common,  
392 higher level, consistent with an accumulate-to-bound process. In the caudate nucleus, the  
393 ramping activity does not converge to a common, higher level. For the first STN subpopulation  
394 (Figure 3), the ramping activity showed on average positive coherence modulation and negative  
395 RT modulation (opposite to predictions of an accumulate-to-bound process) before converging to  
396 a common, higher level. The second STN subpopulation did not show choice-selective activity  
397 before saccade onset. These differences suggest that the caudate and STN neurons participate in  
398 decision deliberation but do not directly mediate decision termination (bound crossing). It is also  
399 possible that the ramping activity reflects some roles for the STN in the evaluation of the  
400 decision process, the tracking of elapsed time, or both. How these possible roles relate to those of  
401 caudate neurons awaits further investigation (Fan et al., 2024).

402 Third, whereas unilateral perturbations in LIP and SC tend to induce contralateral choice biases  
403 (Hanks et al., 2006; Jun et al., 2021; Jeurissen et al., 2022; Stine et al., 2023), unilateral STN  
404 (and caudate) microstimulation can induce both contralateral and ipsilateral choice biases,  
405 depending on the stimulation site (Ding and Gold, 2012b; Doi et al., 2020). At many sites, STN  
406 microstimulation effects on RT were often bilateral and of the same polarity. Moreover, STN  
407 microstimulation seems to have a particularly strong effect on the overall dependence of choice  
408 and RT on evidence, which was not the case for other oculomotor regions. These differences  
409 suggest that the STN has unique roles in choice-independent computations, potentially including  
410 those involving evidence pooled for all alternatives or general bound dynamics (Bogacz and  
411 Gurney, 2007; Ratcliff and Frank, 2012).

412 In summary, we characterized single-neuron activity and the effects of local perturbations in the  
413 STN of monkeys performing a deliberative visual-oculomotor decision task. Our results  
414 validated key aspects of previous theoretical predictions, providing experimental evidence for the

415 multiple involvement in modulating decision deliberation and commitment. Our results also  
416 identified other features of decision-related processing in STN that differ from both theoretical  
417 predictions and known properties of other brain areas that contribute to these kinds of decisions.  
418 These differences can help guide future investigations that aim to delineate how cortical-  
419 subcortical interactions in general, and interactions involving the STN in particular, support  
420 decision-making and other aspects of higher brain function.

421

## 422 **Methods**

423 For this study, we used two adult male rhesus monkeys (*Macaca mulatta*) that have been  
424 extensively trained on the direction-discrimination (dots) task. All training, surgery, and  
425 experimental procedures were in accordance with the National Institutes of Health Guide for the  
426 Care and Use of Laboratory Animals and were approved by the University of Pennsylvania  
427 Institutional Animal Care and Use Committee (protocol # 804726).

### 428 Task design and electrophysiology

429 The behavioral task (Figure 1A), general surgical procedure, and data acquisition methods have  
430 been described in detail previously (Ding and Gold, 2010, 2012b). Briefly, the monkey was  
431 required to report the perceived motion direction of the random-dot stimulus with a saccade at a  
432 self-determined time. Trials with different motion coherences (drawn from five levels) and  
433 directions were interleaved randomly. The monkey's eye position was monitored with a video-  
434 based eye tracker and provided reward/error feedback online based on comparisons between the  
435 monkey's eye position and task-relevant locations. Saccade reaction time (RT) was measured  
436 offline with established velocity and acceleration criteria. Neural activity was recorded using  
437 glass-coated tungsten electrodes (Alpha-Omega) or polyamide-coated tungsten electrodes (FHC,  
438 Inc.), using a grid system through a recording chamber with access to the STN. For  
439 microstimulation sessions, lower-impedance FHC electrodes were used to record and stimulate at  
440 the same sites. Single units were identified by offline spike sorting (Offline Sorter, Plexon, Inc.).  
441 Electrical microstimulation was delivered using Grass S88 stimulator as a train of negative-  
442 leading bipolar current pulses (250  $\mu$ s pulse duration, 200 Hz) from motion onset to saccade  
443 onset. For most sessions, a current intensity of 50  $\mu$ A was used. In other sessions, we lowered the  
444 intensity to ensure that microstimulation did not abolish the monkey's ability to complete the  
445 trials. We randomly interleaved trials with and without microstimulation at a 1:1 ratio.

### 446 Localizing the STN

447 We obtained structural MRI scans using T1- MPRAGE and/or T2-SPACE sequences. We  
448 estimated the likely chamber coordinates with access to the STN from these images (and 3D  
449 reconstruction using BrainSight from Rogue Research, Inc) and mapped the surrounding areas  
450 electrophysiologically. Specifically, we identified several putative landmark regions, including 1)  
451 thalamus, which showed characteristic bursts of activity in a low-firing background while the  
452 monkey dozed off; 2) reticular nucleus of the thalamus, where neurons exhibited high baseline  
453 firing rates (with bursts sometimes > 100Hz); 3) zona incerta, where neurons exhibited low, tonic

454 baseline firing and briefly paused their activity around saccades (Ma, 1996); 4) substantia nigra,  
455 pars reticulata, where some neurons showed high baseline firing rates and suppression in activity  
456 around visual stimulus or saccade onset (Hikosaka and Wurtz, 1983); and 5) substantia nigra,  
457 pars compacta, where neurons showed low baseline firing and responded to unexpected reward.  
458 Based on a macaque brain atlas (Saleem and Logothetis, 2007) and previously reported STN  
459 activity patterns (Matsumura et al., 1992; Wichmann et al., 1994b; Isoda and Hikosaka, 2008),  
460 we defined STN as the area that: 1) was surrounded by these landmark regions, 2) was separated  
461 from them by gaps with minimal activity (white matter), and 3) exhibited irregular firing patterns  
462 with occasional short bursts. The baseline firing rate, measured within 50 ms before fixation  
463 point onset, had a mean±SD magnitude of 15.4±12.4 spikes/s in our sample.

#### 464 Neural-activity analysis

465 We measured the firing rates for each neuron and trial condition in running windows (300 ms)  
466 aligned to motion and saccade onsets. To visualize the overall activation/suppression, we  
467 averaged the firing rates across trial conditions and computed the z-scores using a 300 ms  
468 window before motion onset as the baseline. To visualize the overall choice preferences, we  
469 averaged the firing rates for each choice, computed the difference between choices, and z-scored  
470 the difference using the same baseline window. To quantitatively measure each neuron's task-  
471 related modulation, we performed two multiple linear regressions for each running window,  
472 separately for coherence and RT because monkeys' RT strongly depends on coherence on our  
473 task:

$$474 \text{ Spike count} = \beta_0 + \beta_{\text{Choice}} \times I_{\text{Choice}} + \beta_{\text{Coh-Contra}} \times I_{\text{Coh-Contra}} + \beta_{\text{Coh-Ipsi}} \times I_{\text{Coh-Ipsi}}$$

475 (Eq. 1)

$$476 \text{ Spike count} = \beta_0 + \beta_{\text{Choice}} \times I_{\text{Choice}} + \beta_{\text{RT-Contra}} \times I_{\text{RT-Contra}} + \beta_{\text{RT-Ipsi}} \times I_{\text{RT-Ipsi}}$$

477 (Eq. 2)

478 where  $I_{\text{Choice}} = \{1 \text{ for contralateral choice, } -1 \text{ for ipsilateral choice}\}$ ,

479  $I_{\text{Coh-Contra}} = \{\text{coherence for contralateral choice, } 0 \text{ for ipsilateral choice}\}$ ,

480  $I_{\text{Coh-Ipsi}} = \{0 \text{ for contralateral choice, coherence for ipsilateral choice}\}$ .

481  $I_{\text{RT-Contra}} = \{\text{RT for contralateral choice, } 0 \text{ for ipsilateral choice}\}$ ,

482  $I_{\text{RT-Ipsi}} = \{0 \text{ for contralateral choice, RT for ipsilateral choice}\}$ .

483 Contralateral/ipsilateral choices refer to saccades toward the target contralateral/ipsilateral to the  
484 recording sites. Significance of non-zero coefficients was assessed using a *t*-test (criterion:  $p =$   
485 0.05).

486

#### 487 Cluster analysis

488 We converted each neuron's activity into a 30-D vector consisting of the average firing rate  
489 within three 200-ms windows for all trial conditions (i.e., 2 choices  $\times$  5 coherence levels). The  
490 windows were selected as early motion viewing (100 – 300 ms after motion onset), late motion  
491 viewing (300 – 500 ms after motion onset), and peri-saccade (100 ms before to after saccade

492 onset). The choice identity was designated as either “preferred” and “other”, based on the  
493 relative average activity in the peri-saccade window. Note that this designation was used so that  
494 neurons with similar general modulation patterns except for the polarity of their choice  
495 selectivity would be grouped together. This designation was not based on any statistical test and  
496 did not imply that the peri-saccade activity was reliably choice selective. The average firing rate  
497 for each neuron was then z-scored based on baseline rates measured in a 300 ms window ending  
498 at motion onset.

499 We explored multiple method variations using k-means clustering and present results from the  
500 variation with the highest stability. These variations included: 1) whether or not the vectors were  
501 projected onto 11 principal components that together explained at least 95% of total variance;  
502 and 2) calculation of vector distance, including squared Euclidean, cosine, and correlation  
503 metrics. We determined the best settings using: 1) the Rand index (Rand, 1971), which quantifies  
504 the stability of clusters in repeated clustering; 2) Silhouette scores, which quantifies the quality  
505 of grouping and separation between clusters; and 3) visual inspection of clustering results in  
506 terms of both cluster distribution in a t-SNE space and average activity of the clusters. To  
507 compute the Rand index, we performed 50 runs of clustering, assuming 3-9 clusters, for each  
508 combination of variations. The Rand index was computed as the fraction of consistent grouping  
509 between a pair of units between two clustering runs. For two runs of clustering results, Rand  
510 index =  $\frac{N_{same-same} + N_{different-different}}{N_{all\ pairs}}$ , where  $N_{same-same}$  counts the number of neuron pairs that  
511 share clusters in both runs,  $N_{different-different}$  counts the number of neuron pairs that do not  
512 share clusters in either run, and  $N_{all\ pairs}$  counts the total number of neuron pairs. To compute  
513 the Silhouette scores, we chose the best of 100 repetitions of clustering for each combination of  
514 variations. For each neuron, Silhouette score =  $\frac{\max(D_{inter-cluster}, D_{intra-cluster})}{D_{inter-cluster} - D_{intra-cluster}}$ , where  
515  $D_{inter-cluster}$  is the average distance to the neuron’s nearest neighboring cluster, and  
516  $D_{intra-cluster}$  is the average distance to other neurons in the same cluster. A positive score  
517 implies that, for the given neuron, its activity was more similar to other neurons within the same  
518 cluster than those in its nearest neighboring cluster. A negative score implies that the neuron’s  
519 activity was more similar to those outside its own cluster.

520 To classify activity recorded at a microstimulation site, we calculated the correlation between its  
521 30-D vector and the centroids from random-seeded clustering. The centroid with the highest  
522 correlation value determined the cluster identity of the activity.

### 523 Microstimulation-effects analysis

524 We analyzed microstimulation effects in several ways. To characterize the effects without  
525 assumptions about the underlying decision process, we fitted logistic functions to the choice data  
526 and linear functions to the RT data. We used three variants of the logistic functions that differed  
527 in their use of lapse rates, which measure the probability of errors independent of motion  
528 strength:

529 No Lapse:  $p$  (contralateral choice) =  $\frac{1}{1 + e^{-(Slope_0 + Slope_{estim}) \times (Coh + Bias_0 + Bias_{estim})}}$  (Eq. 3)

530 Symmetric Lapse:  $p$  (*contralateral choice*) =  $\lambda_0 + \lambda_{estim} +$   
 531 
$$\frac{1 - 2 \times (\lambda_0 + \lambda_{estim})}{1 + e^{-(Slope_0 + Slope_{estim}) \times (Coh + Bias_0 + Bias_{estim})}}$$
 (Eq. 4)

532 Asymmetric Lapse:  $p$  (*contralateral choice*) =  $\lambda_{Ipsi0} + \lambda_{Ipsi-estim} +$   
 533 
$$\frac{1 - \lambda_{Ipsi0} - \lambda_{Ipsi-estim} - \lambda_{Contra0} - \lambda_{Contra-estim}}{1 + e^{-(Slope_0 + Slope_{estim}) \times (Coh + Bias_0 + Bias_{estim})}}$$
 (Eq. 5)

534 where Coh is the signed coherence (positive/negative for motion toward the  
 535 contralateral/ipsilateral choice). Contralateral/ipsilateral choices refer to saccades toward the  
 536 targets contralateral/ipsilateral to the microstimulation sites, respectively. To assess the  
 537 significance of the “estim” terms, we used bootstrap methods. Specifically, we generated 200  
 538 sets of data by shuffling the microstimulation status of trials within each session. We fitted these  
 539 artificial data using the same logistic functions to estimate null distributions for each parameter  
 540 and performed a one-tailed test to determine if the actual fit value exceeded chance (criterion,  $p$   
 541  $< 0.05$ ).

542 We fitted linear functions to the RT data, separately for the two choices:

543 
$$RT = Offset_0 + Offset_{estim} + (Slope_0 + Slope_{estim}) \times Coh_{unsigned}$$
 (Eq. 6)

544 We assessed significance using  $t$ -tests (criterion,  $p < 0.05$ ).

545 To infer microstimulation effects on decision-related computations, we fitted drift-diffusion  
 546 models to choice and RT data simultaneously. We used DDM variants with collapsing bounds  
 547 (DDM; Figure 7A), following previously established procedures (Fan et al., 2018; Doi et al.,  
 548 2020). Briefly, the DDM assumes that motion evidence is accumulated over time into a decision  
 549 variable (DV), which is compared to two collapsing choice bounds. A choice is made when the  
 550 DV crosses either bound, such that the time of crossing determines the decision time and the  
 551 identity of the bound determines the choice identity. The model has eight basic parameters  
 552 (presented here in six groups): 1)  $a$ , the maximal bound height; 2)  $B_{collapse}$  and  $B_t$ , the decay  
 553 speed and onset specifying the time course of the bound “collapse”; 3)  $k$ , a scale factor governing  
 554 the rate of evidence accumulation; 4)  $me$ , an offset specifying a bias in the rate of evidence  
 555 accumulation; 5)  $z$ , an offset specifying a bias in the DV, or equivalently, asymmetric offsets of  
 556 equal magnitude for the two choice bounds; and 6)  $t0_{contra}$  and  $t0_{ipsi}$ , non-decision times for  
 557 the two choices that capture RT components that do not depend on evidence accumulation (e.g.,  
 558 visual latency and motor delay).

559 We used 8 variants of DDM. In the Full model, all eight parameters were allowed to change with  
 560 microstimulation. In the None model, all eight parameters did not change with microstimulation.  
 561 In six reduced models (NoA, NoCollapse, NoK, NoME, NoZ, NoT), the corresponding group of  
 562 parameters (specified above) were fixed while the other parameters were allowed to change with  
 563 microstimulation. We fitted each model using the maximum *a posteriori* estimate method and  
 564 previously established prior distributions (Wiecki et al., 2013). We performed five runs for each  
 565 fit and used the best run (highest likelihood) for analyses here. We used the Akaike Information  
 566 Criterion (AIC) for model selection. We considered an AIC difference  $>3$  to indicate that the  
 567 smaller-AIC model significantly outperformed the larger-AIC model. For a given sessions, if the

568 Full model outperformed a reduced model and the None model, we considered that session to  
569 show significant microstimulation effect(s) on the corresponding model parameter(s). For  
570 example, we considered STN microstimulation to induce significant changes in  $k$  if the Full  
571 model outperformed both None and NoK models for a given session.

572 **Acknowledgements**

573 We thank Jean Zweigle for outstanding animal care and training, Lowell Thompson and Kara  
574 McGaughey for comments on the manuscript, and Michael Suplick for machine shop support  
575 (NIH National Eye Institute Core Grant P30 EY001583). This work was supported by NIH  
576 National Eye Institute (R01-EY022411; LD and JIG).

577

578 **Author contributions**

579 Conceptualization, LD and JIG; methodology, KR and LD; investigation, KR and LD;  
580 visualization, LD and JIG; funding acquisition, LD and JIG; project administration, LD;  
581 supervision, LD; writing – original draft, LD; writing – review & editing, KR, JIG, and LD.

582

583 **Declaration of interests**

584 The authors declare no competing financial interests.

585



## 586 **Figure Legends**

587 **Figure 1. Behavioral task and model predictions.** A, Behavioral task. The monkey was  
588 required to report the perceived motion direction of the random-dot stimulus by making a  
589 saccade towards the corresponding choice target at a self-determined time. B, Three previous  
590 models predicted different patterns of STN activity. Sensitive to choice: differential responses for  
591 trials ending with different choices. Sensitive to uncertainty: differential responses for trials with  
592 different evidence strength.

593 **Figure 2. STN neurons have diverse response profiles.** A, Activity of three STN neurons  
594 (rows) aligned to motion (left) and saccade (right) onsets and grouped by choice  $\times$  motion  
595 coherence (see legend). For motion-onset alignment, activity was truncated at 100 ms before  
596 saccade onset. For saccade-onset alignment, activity was truncated before 200 ms after motion  
597 onset. B, Summary of average activity patterns. Each row represents the activity of a neuron, z-  
598 scored by baseline activity in a 300 ms window before target onset and averaged across all trial  
599 conditions. Rows are grouped by monkey (red and green shown to the right of each panel:  
600 monkeys C and F, respectively) and sorted by the time of peak values relative to motion onset.  
601 Only correct trials were included. C, Heatmaps of linear regression coefficients for choice (top),  
602 coherence for trials with contralateral choices (middle), and coherence for trials with ipsilateral  
603 choices (bottom), for activity aligned to motion (left) and saccade (right) onsets. Regression was  
604 performed in running windows of 300 ms. Regression coefficients that were not significantly  
605 different from zero ( $t$ -test,  $p > 0.05$ ) were set to zero (green) for display purposes. Neurons were  
606 sorted in rows by the time of peak coefficient magnitude. Only correct trials were included. D,  
607 Time courses of the fractions of regression coefficients that were significantly different from zero  
608 ( $t$ -test,  $p < 0.05$ ), for choice (black), coherence for trials with contralateral choices (red), and  
609 coherence for trials with ipsilateral choices (blue). Dashed line indicates chance level. E, Time  
610 courses of the fractions of non-zero regression coefficients for coherence. Separate fractions  
611 were calculated for trials with the preferred (purple) and null (green) choices from choice-  
612 selectivity activity and for all trials from activity that was not choice selective (gray). Only time  
613 points after motion onset with fractions  $> 0.05$  for choice-selective activity were included.  
614 Dashed line indicates chance level.

615 **Figure 3. STN contains distinct subpopulations.** A, Three activity vectors that were  
616 constructed based on theoretical predictions in Figure 1B and used as seeds for  $k$ -means  
617 clustering (see Methods). B, Each panel shows the average activity of neurons in a cluster, same  
618 format as Figure 2A. The numbers indicate the cluster size. C, Visualization of the clusters using  
619 the  $t$ -distributed stochastic neighbor embedding ( $t$ -SNE) dimension-reduction method. D,  
620 Average activity of clusters identified using random-seeded  $k$ -means clustering. Same format as  
621 Figure 3B. E, Visualization of the random-seeded clusters in the same tSNE space.

622 **Figure 4. Clustering parameters.** A, Silhouette plots for clustering results using different  
623 combinations of settings. Silhouette scores for neurons are grouped by clusters and sorted. Red  
624 lines indicate the mean scores. Yellow shaded box indicates the chosen setting for results in  
625 Figure 3. B, Average Rand indices for different clustering settings. For each setting, the  $k$ -means  
626 algorithm was run 50 times, each time picking the best clusters out of 100 repetitions. Higher

627 Rand index indicates greater cluster stability across different runs. Blue box indicates settings  
628 with Rand indices  $> 0.95$ . C, Mean silhouette scores and the number of negative scores as a  
629 function of number of clusters, using the firing rate vectors and correlation distance. Higher  
630 mean score and fewer negative scores indicate better clustering.

631 **Figure 5. STN microstimulation affects monkeys' choice and RT.** A-C, Monkey's choice (top)  
632 and RT (bottom) performance for trials with (red) and without (black) microstimulation for three  
633 example sessions (A,B: two sites in monkey C; C: monkey F). Lines: DDM fits. D, Distributions  
634 of microstimulation effects on bias and slope terms of the logistic function. Filled bars in  
635 histograms indicate sessions with significant modulation of the specific term (bootstrap method).  
636 Triangles indicate the median values. Filled triangle: Wilcoxon sign-rank test for  $H_0$ : median=0,  
637  $p < 0.05$ . E and F, Summary of microstimulation effects on the offset (E) and slope (F) terms of a  
638 linear regression fit to RT data. Two separate linear regressions were performed for the two  
639 choices (Ipsi/Contra, as indicated). Triangles indicate the median values. Filled triangles:  
640 Wilcoxon sign-rank test,  $p < 0.05$ .

641 **Figure 6. STN microstimulation affected multiple computational components in the DDM.**  
642 A, Illustration of the DDM. Red/black lines represent across-trial mean/single-trial example of  
643 the evidence (top) and drift rate (bottom). Blue lines represent the collapsing decision bounds. B,  
644 Distribution of the difference in AIC between the None and Full models. Red dashed line  
645 indicates the criterion for choosing the full model: AIC difference = 3. C, Histograms of  
646 microstimulation effects on DDM parameters. Each histogram included only sessions in which  
647 the Full model outperformed the corresponding reduced model (e.g., the histogram for parameter  
648  $a$  included only sessions in which  $AIC_{NoA} - AIC_{Full} > 3$  and  $AIC_{None} - AIC_{Full} > 3$ ). Triangles  
649 indicate median values. Filled triangles: Wilcoxon sign rank test,  $p < 0.05$ . D, Summary of  
650 microstimulation effects on all parameters, for sessions in which at least one significant effect  
651 was present. Sessions were sorted by the prevalence and sign of the effects.

652 **Figure 7. Different STN subpopulations are intermingled.** Locations of STN neurons, color-  
653 coded by clusters based on random-seed clustering (same as Figure 3D). The Medial-Lateral  
654 (ML) values were jittered for better visualization of neurons recorded along the same track and at  
655 similar depths. Anterior-Posterior (AP) levels were relative to the anterior commissure. ML and  
656 depth levels were relative to the center of the recording chambers.

657 **Figure 8. STN microstimulation effects depend partially on neural clusters.** A, Average  
658 activity at stimulation sites, grouped by four clusters based on the clusters in Figure 3D. B,  
659 Fractions of significant microstimulation effects for sites with the presence of each neuron  
660 cluster. Significance was based on AIC comparison between reduced and Full models. C,  
661 Microstimulation effects grouped by neuron cluster. Same format as Figure 5D. D, Fractions of  
662 significant microstimulation effects, grouped by effects reflecting changes in bound, decision  
663 variable computation, and non-decision processes.

## 664 Supplemental Information

665 **Suppl. Figure 1. STN activity is modulated by choice and RT.** Same format as Figure 2,  
666 except using choice and RT as regressors.

667 **Suppl. Figure 2. Summary of regression results, separated for different subpopulations.**

668 A: fractions of neurons in each category that showed significant modulation (t-test,  
669  $p < 0.05$ ) at each time window by choice (top), coherence for trials with contralateral choices  
670 (middle), and coherence for trials with ipsilateral choices (bottom). Dashed horizontal lines  
671 indicate the 5% chance level. Colors indicate categories as in Figure 3. B: median values  
672 of regression coefficients for choice and coherence as a function of time.

673 **Suppl. Figure 3. Clustering results using alternative numbers of clusters, visualized in tSNE**  
674 **space.** Same format as Figure 3E.

675 **Suppl. Figure 4. Clustering results using alternative numbers of clusters, visualized as**  
676 **average firing rates for each cluster.** Same format as Figure 3B and D.

677 **Suppl. Figure 5. Comparison of different logistic models.** A, The No Lapse model was  
678 associated with the lowest AIC for most sessions. The Symmetric Lapse model was associated  
679 with lower AICs for 12 sessions. The Asymmetric Lapse model was associated with lower AICs  
680 for 8 sessions. B, Histograms of microstimulation effects on bias, slope, and lapse terms in the  
681 Symmetric Lapse model. C, Histograms of microstimulation effects on bias, slope, and two lapse  
682 (for each choice) terms in the Asymmetric Lapse model. Same format as the histograms in Figure  
683 5D.

684 **Suppl. Figure 6.** A, Differences in AIC between reduced and Full models. Filled circles indicate  
685 sessions for which  $AIC_{\text{Reduced}} - AIC_{\text{Full}} > 3$  (red line). Note that for three sessions, the Full model  
686 outperformed the None model but not any of the reduced models. B, Histograms of difference in  
687 DDM parameters between trials with and without microstimulation. Filled bars represent  
688 sessions considered to show significant microstimulation effects on the given parameter, based  
689 on AIC comparisons. Triangles indicate median values. Filled triangles: Wilcoxon sign-rank test,  
690  $p < 0.05$ .

691 **Suppl. Figure 7. Indices of motivational state did not differ among sessions with different**  
692 **neuron subpopulations.** Panels show the summary of rate of fixation break (left), overall error  
693 rate (middle) and mean RT (right) for the four categories identified in Figure 3. All indices were  
694 z-scored across sessions for each monkey. Red lines indicate median values. The bottom and top  
695 edges of the box indicate the 25th and 75th percentiles, respectively. The whiskers extend to the  
696 most extreme data points not considered outliers, and the outliers are plotted individually as dots.  
697 ANOVA,  $p = 0.06, 0.91,$  and  $0.29,$  respectively. No significant difference was observed for each  
698 monkey separately ( $p > 0.08$  and  $0.12$  for all indices for monkeys C and F, respectively).

699

700 **Suppl Table 1. Indices of motivational state did not correlate with microstimulation effects.**

701 P values are raw values from Pearson correlation, not corrected for multiple testing.

702

DDM components	Fixation Break		Error Rate		Mean RT	
	Correlation	p Value	Correlation	p Value	Correlation	p Value
B_d	-0.018	0.897	0.098	0.481	0.134	0.335
B_alpha	-0.070	0.615	0.075	0.591	-0.314	0.021
a	-0.049	0.723	-0.046	0.739	0.013	0.927
k	0.236	0.085	0.149	0.283	0.223	0.105
me	0.057	0.680	-0.027	0.844	0.035	0.802
z	-0.260	0.057	-0.031	0.822	0.041	0.768
T0_ipsi	0.205	0.138	0.049	0.724	0.166	0.231
T0_contra	0.060	0.669	-0.010	0.941	0.270	0.048

703

## 704 **References**

- 705 Aron AR, Behrens TE, Smith S, Frank MJ, Poldrack RA (2007) Triangulating a cognitive control  
706 network using diffusion-weighted magnetic resonance imaging (MRI) and functional  
707 MRI. *J Neurosci Off J Soc Neurosci* 27:3743–3752.
- 708 Aron AR, Poldrack RA (2006) Cortical and subcortical contributions to Stop signal response  
709 inhibition: role of the subthalamic nucleus. *J Neurosci* 26:2424–2433.
- 710 Baunez C, Humby T, Eagle DM, Ryan LJ, Dunnett SB, Robbins TW (2001) Effects of STN  
711 lesions on simple vs choice reaction time tasks in the rat: preserved motor readiness, but  
712 impaired response selection. *Eur J Neurosci* 13:1609–1616.
- 713 Bergman H, Wichmann T, DeLong MR (1990) Reversal of experimental parkinsonism by lesions  
714 of the subthalamic nucleus. *Science* 249:1436–1438.
- 715 Bergman H, Wichmann T, Karmon B, DeLong MR (1994) The primate subthalamic nucleus. II.  
716 Neuronal activity in the MPTP model of parkinsonism. *J Neurophysiol* 72:507–520.
- 717 Bogacz R, Gurney K (2007) The basal ganglia and cortex implement optimal decision making  
718 between alternative actions. *Neural Comput* 19:442–477.
- 719 Brittain J-S, Watkins KE, Joundi RA, Ray NJ, Holland P, Green AL, Aziz TZ, Jenkinson N  
720 (2012) A role for the subthalamic nucleus in response inhibition during conflict. *J*  
721 *Neurosci* 32:13396–13401.
- 722 Carpenter MB, Whittier JR, Mettler FA (1950) Analysis of choreoid hyperkinesia in the Rhesus  
723 monkey; surgical and pharmacological analysis of hyperkinesia resulting from lesions in  
724 the subthalamic nucleus of Luys. *J Comp Neurol* 92:293–331.
- 725 Cavanagh JF, Wiecki TV, Cohen MX, Figueroa CM, Samanta J, Sherman SJ, Frank MJ (2011)  
726 Subthalamic nucleus stimulation reverses mediofrontal influence over decision threshold.  
727 *Nat Neurosci* 14:1462–1467.
- 728 Cho S-H, Crapse T, Grimaldi P, Lau H, Basso MA (2021) Variable Statistical Structure of  
729 Neuronal Spike Trains in Monkey Superior Colliculus. *J Neurosci* 41:3234–3253.
- 730 Coulthard EJ, Bogacz R, Javed S, Mooney LK, Murphy G, Keeley S, Whone AL (2012) Distinct  
731 roles of dopamine and subthalamic nucleus in learning and probabilistic decision making.  
732 *Brain*.
- 733 Crapse TB, Lau H, Basso MA (2018) A Role for the Superior Colliculus in Decision Criteria.  
734 *Neuron* 97:181-194.e6.
- 735 DeLong MR, Crutcher MD, Georgopoulos AP (1985) Primate globus pallidus and subthalamic  
736 nucleus: functional organization. *J Neurophysiol* 53:530–543.

- 737 DeLong MR, Wichmann T (2001) Deep brain stimulation for Parkinson's disease. *Ann Neurol*  
738 49:142–143.
- 739 Desbonnet L, Temel Y, Visser-Vandewalle V, Blokland A, Hornikx V, Steinbusch HWM (2004)  
740 Premature responding following bilateral stimulation of the rat subthalamic nucleus is  
741 amplitude and frequency dependent. *Brain Res* 1008:198–204.
- 742 Ding L, Gold JI (2010) Caudate encodes multiple computations for perceptual decisions. *J*  
743 *Neurosci* 30:15747–15759.
- 744 Ding L, Gold JI (2012a) Neural correlates of perceptual decision making before, during, and  
745 after decision commitment in monkey frontal eye field. *Cereb Cortex* 22:1052–1067.
- 746 Ding L, Gold JI (2012b) Separate, causal roles of the caudate in saccadic choice and execution in  
747 a perceptual decision task. *Neuron* 75:865–874.
- 748 Doi T, Fan Y, Gold JI, Ding L (2020) The caudate nucleus contributes causally to decisions that  
749 balance reward and uncertain visual information. *Elife* 9:e56694.
- 750 Fan Y, Doi T, Gold JI, Ding L (2024) Neural Representations of Post-Decision Accuracy and  
751 Reward Expectation in the Caudate Nucleus and Frontal Eye Field. *J Neurosci* 44.
- 752 Fan Y, Gold JI, Ding L (2018) Ongoing, rational calibration of reward-driven perceptual biases.  
753 *Elife* 7:e36018.
- 754 Fan Y, Gold JI, Ding L (2020) Frontal eye field and caudate neurons make different contributions  
755 to reward-biased perceptual decisions. *eLife* 9:e60535.
- 756 Frank MJ (2006) Hold your horses: a dynamic computational role for the subthalamic nucleus in  
757 decision making. *Neural Netw* 19:1120–1136.
- 758 Frank MJ, Samanta J, Moustafa AA, Sherman SJ (2007) Hold your horses: impulsivity, deep  
759 brain stimulation, and medication in parkinsonism. *Science* 318:1309–1312.
- 760 Fumagalli M, Giannicola G, Rosa M, Marceglia S, Lucchiari C, Mrakic-Sposta S, Servello D,  
761 Pacchetti C, Porta M, Sassi M, Zangaglia R, Franzini A, Albanese A, Romito L,  
762 Piacentini S, Zago S, Pravettoni G, Barbieri S, Priori A (2011) Conflict-dependent  
763 dynamic of subthalamic nucleus oscillations during moral decisions. *Soc Neurosci*  
764 6:243–256.
- 765 Gold JI, Shadlen MN (2007) The neural basis of decision making. *Annu Rev Neurosci* 30:535–  
766 574.
- 767 Green N, Bogacz R, Huebl J, Beyer AK, Kuhn AA, Heekeren HR (2013) Reduction of influence  
768 of task difficulty on perceptual decision making by STN deep brain stimulation. *Curr*  
769 *Biol* 23:1681–1684.

- 770 Hanks TD, Ditterich J, Shadlen MN (2006) Microstimulation of macaque area LIP affects  
771 decision-making in a motion discrimination task. *Nat Neurosci* 9:682–689.
- 772 Herz DM, Tan H, Brittain JS, Fischer P, Cheeran B, Green AL, FitzGerald J, Aziz TZ, Ashkan K,  
773 Little S, Foltynie T, Limousin P, Zrinzo L, Bogacz R, Brown P (2017) Distinct  
774 mechanisms mediate speed-accuracy adjustments in cortico-subthalamic networks. *Elife*  
775 6.
- 776 Herz DM, Zavala BA, Bogacz R, Brown P (2016) Neural Correlates of Decision Thresholds in  
777 the Human Subthalamic Nucleus. *Curr Biol* 26:916–920.
- 778 Hikosaka O, Wurtz RH (1983) Visual and oculomotor functions of monkey substantia nigra pars  
779 reticulata. III. Memory-contingent visual and saccade responses. *J Neurophysiol*  
780 49:1268–1284.
- 781 Isoda M, Hikosaka O (2008) Role for subthalamic nucleus neurons in switching from automatic  
782 to controlled eye movement. *J Neurosci* 28:7209–7218.
- 783 Jeurissen D, Shushruth S, El-Shamayleh Y, Horwitz GD, Shadlen MN (2022) Deficits in  
784 decision-making induced by parietal cortex inactivation are compensated at two  
785 timescales. *Neuron* 110:1924-1931.e5.
- 786 Jun E, Bautista A, Nunez M, Allen D, Tak J, Alvarez E, Basso M (2021) Causal role for the  
787 primate superior colliculus in the computation of evidence for perceptual decisions. *Nat*  
788 *Neurosci* 24:1121–1131.
- 789 Lehericy S, Ducros M, Krainik A, Francois C, Van de Moortele PF, Ugurbil K, Kim DS (2004)  
790 3-D diffusion tensor axonal tracking shows distinct SMA and pre-SMA projections to the  
791 human striatum. *Cereb Cortex* 14:1302–1309.
- 792 Lo CC, Wang XJ (2006) Cortico-basal ganglia circuit mechanism for a decision threshold in  
793 reaction time tasks. *Nat Neurosci* 9:956–963.
- 794 Ma TP (1996) Saccade-related omnivectoral pause neurons in the primate zona incerta.  
795 *Neuroreport* 7:2713–2716.
- 796 Martin JP (1927) Hemichorea resulting from a local lesion of the brain. (The syndrome of the  
797 body of Luys.). *Brain* 50:637–649.
- 798 Martin JP, Alcock NS (1934) Hemichorea associated with a lesion of the corpus Luysii. *Brain*  
799 57:504–516.
- 800 Matsumura M, Kojima J, Gardiner TW, Hikosaka O (1992) Visual and oculomotor functions of  
801 monkey subthalamic nucleus. *J Neurophysiol* 67:1615–1632.
- 802 Meister ML, Hennig JA, Huk AC (2013) Signal multiplexing and single-neuron computations in  
803 lateral intraparietal area during decision-making. *J Neurosci* 33:2254–2267.

- 804 Nambu A, Takada M, Inase M, Tokuno H (1996) Dual somatotopical representations in the  
805 primate subthalamic nucleus: evidence for ordered but reversed body-map  
806 transformations from the primary motor cortex and the supplementary motor area. *J*  
807 *Neurosci* 16:2671–2683.
- 808 Pagnier GJ, Asaad WF, Frank MJ (2024) Double dissociation of dopamine and subthalamic  
809 nucleus stimulation on effortful cost/benefit decision making. *Curr Biol CB* 34:655-  
810 660.e3.
- 811 Parent A, Hazrati LN (1995) Functional anatomy of the basal ganglia. II. The place of  
812 subthalamic nucleus and external pallidum in basal ganglia circuitry. *Brain Res Brain Res*  
813 *Rev* 20:128–154.
- 814 Pasquereau B, Turner RS (2017) A selective role for ventromedial subthalamic nucleus in  
815 inhibitory control. *Elife* 6.
- 816 Pote I, Torkamani M, Kefalopoulou ZM, Zrinzo L, Limousin-Dowsey P, Foltynie T,  
817 Speekenbrink M, Jahanshahi M (2016) Subthalamic nucleus deep brain stimulation  
818 induces impulsive action when patients with Parkinson’s disease act under speed  
819 pressure. *Exp Brain Res* 234:1837–1848.
- 820 Prasad AA, Wallén-Mackenzie Å (2024) Architecture of the subthalamic nucleus. *Commun Biol*  
821 7:1–14.
- 822 Rand WM (1971) Objective Criteria for the Evaluation of Clustering Methods. *J Am Stat Assoc*  
823 66:846–850.
- 824 Ratcliff R, Frank MJ (2012) Reinforcement-based decision making in corticostriatal circuits:  
825 mutual constraints by neurocomputational and diffusion models. *Neural Comput*  
826 24:1186–1229.
- 827 Redgrave P, Prescott TJ, Gurney K (1999) The basal ganglia: a vertebrate solution to the  
828 selection problem? *Neuroscience* 89:1009–1023.
- 829 Roitman JD, Shadlen MN (2002) Response of neurons in the lateral intraparietal area during a  
830 combined visual discrimination reaction time task. *J Neurosci* 22:9475–9489.
- 831 Saleem KS, Logothetis N (2007) A combined MRI and histology atlas of the rhesus monkey  
832 brain in stereotaxic coordinates. London ; Burlington, MA: Academic.
- 833 Schmidt R, Leventhal DK, Mallet N, Chen F, Berke JD (2013) Canceling actions involves a race  
834 between basal ganglia pathways. *Nat Neurosci* 16:1118–1124.
- 835 Stine GM, Trautmann EM, Jeurissen D, Shadlen MN (2023) A neural mechanism for terminating  
836 decisions. *Neuron* 111:2601-2613.e5.
- 837 Tehovnik EJ (1996) Electrical stimulation of neural tissue to evoke behavioral responses. *J*  
838 *Neurosci Methods* 65:1–17.



- 839 Wei W, Rubin JE, Wang XJ (2015) Role of the indirect pathway of the basal ganglia in  
840 perceptual decision making. *J Neurosci* 35:4052–4064.
- 841 Whittier JR, Mettler FA (1949) Studies on the subthalamus of the rhesus monkey; hyperkinesia  
842 and other physiologic effects of subthalamic lesions; with special reference to the  
843 subthalamic nucleus of Luys. *J Comp Neurol* 90:319–372.
- 844 Wichmann T, Bergman H, DeLong MR (1994a) The primate subthalamic nucleus. III. Changes  
845 in motor behavior and neuronal activity in the internal pallidum induced by subthalamic  
846 inactivation in the MPTP model of parkinsonism. *J Neurophysiol* 72:521–530.
- 847 Wichmann T, Bergman H, DeLong MR (1994b) The primate subthalamic nucleus. I. Functional  
848 properties in intact animals. *J Neurophysiol* 72:494–506.
- 849 Witt K, Pulkowski U, Herzog J, Lorenz D, Hamel W, Deuschl G, Krack P (2004) Deep brain  
850 stimulation of the subthalamic nucleus improves cognitive flexibility but impairs  
851 response inhibition in Parkinson disease. *Arch Neurol* 61:697–700.
- 852 Zaghoul KA, Weidemann CT, Lega BC, Jaggi JL, Baltuch GH, Kahana MJ (2012) Neuronal  
853 Activity in the Human Subthalamic Nucleus Encodes Decision Conflict during Action  
854 Selection. *J Neurosci* 32:2453–2460.
- 855 Zavala B, Damera S, Dong JW, Lungu C, Brown P, Zaghoul KA (2017) Human Subthalamic  
856 Nucleus Theta and Beta Oscillations Entrain Neuronal Firing During Sensorimotor  
857 Conflict. *Cereb Cortex* 27:496–508.
- 858 Zavala BA, Tan H, Little S, Ashkan K, Hariz M, Foltynie T, Zrinzo L, Zaghoul KA, Brown P  
859 (2014) Midline Frontal Cortex Low-Frequency Activity Drives Subthalamic Nucleus  
860 Oscillations during Conflict. *J Neurosci* 34:7322.
- 861